Clim Dyn (2016) 46:3725–3736
DOI 10.1007/s00382-015-2799-3

Threshold of the volcanic forcing that leads the El Niño-like warming in the last millennium: results from the ERIK simulation

Hyung-Gyu Lim[1] · Sang-Wook Yeh[2] · Jong-Seong Kug[1] · Young-Gyu Park[3] · Jae-Hun Park[3,4] · Rokjin Park[5] · Chang-Keun Song[6]

Received: 5 December 2014 / Accepted: 8 August 2015 / Published online: 29 August 2015

Abstract In order to examine the threshold of the volcanic forcing that leads to the El Niño-like warming, we analyze a millennium ERIK simulation (AD 1000–1850) forced by three external forcings including greenhouse gases, solar forcing and volcanic eruptions using the ECHO-G coupled climate model. It is found that there exists a threshold of the volcanic forcing above 15 W/m^2 to lead the El Niño-like warming in the climate model. When the volcanic forcing is above this threshold forcing, then the intensity of the Inter-tropical Convergence Zone (ITCZ) is weakened and its position is shifted to the south. This might be associated with the processes of less evaporation in the subtropical cloudless region by a cooling due to the reduction of net surface shortwave radiation. Concurrently, a weakening of ITCZ is associated with a weakening of the trade winds and the subsequent Bjerknes feedback causes El Niño-like warming. Therefore, El Niño-like warming events can occur when volcanic eruption is above threshold forcing, implying that there exists a certain level of radiative forcing change which is capable of changing the state of tropical Pacific sea surface temperature. The last millennium simulation of Paleoclimate Modeling Intercomparison Project Phase 3 climate models also indicates that there may exist a threshold forcing to lead the El Niño-like warming, which has been also discussed in the present study.

✉ Sang-Wook Yeh
swyeh@hanyang.ac.kr

[1] School of Environmental Science and Engineering, POSTECH, Pohang, Korea

[2] Department of Marine Sciences and Convergent Technology, Hanyang University, Ansan, Korea

[3] Physical Oceanography Division, KIOST, Ansan, Korea

[4] Department of Ocean Sciences, Inha University, Incheon, Korea

[5] School of Earth and Environmental Sciences, Seoul National University, Seoul, Korea

[6] Department of Climate and Air Quality, National Institute of Environmental Research, Incheon, Korea

1 Introduction

The El Niño and Southern Oscillation (ENSO), which influences the global climate through atmospheric teleconnections (Lau 1997; Alexander et al. 2002), is the most dominant variability on Earth on an interannual timescale (McPhaden et al. 2006). Therefore, understanding the ENSO is essential for predicting the weather and climate variability over the globe. A number of theories to explain ENSO development have been developed since the 1960s (Bjerknes 1969; Schopf and Suarez 1988; Suarez and Schopf 1988; Battisti and Hirst 1989; Jin 1997; Picaut et al. 1997; Vimont et al. 2001; Burgers et al. 2005; Vecchi et al. 2006) and there is an agreement to some extent that the atmosphere-to-ocean coupling processes are essential physical processes to explain ENSO development.

In addition, several studies have suggested that solar irradiance and volcanic forcings play a role in initiating the anomalous warm/cold sea surface temperature (SST) in the tropical Pacific through feedback processes (Meehl et al. 2003; van Loon et al. 2004, 2007; van Loon and Meehl 2008; Meehl et al. 2008, 2009). For example, the difference in the solar irradiance between solar maxima and minima years can cause a La Niña-like cooling state. In other words, increased incoming solar radiation inputs greater energy into the subtropical ocean where the amount of cloud is less. Consequently, more moisture is evaporated into the atmosphere and the trade winds carry more moisture into the Inter-tropical Convergence Zone (ITCZ). This

causes an intensified convection along the ITCZ, which induces stronger trade winds. Concurrently, it accompanies the enhanced upwelling intensity in the eastern tropical Pacific, leading to the La Niña-like cooling state.

On the other hand, volcanic eruption can also modulate the atmospheric radiative forcings and cause them to reach the surface by changing the amount of incoming solar radiation (Robock and Mao 1995; D'Arrigo et al. 2009). Explosive volcanic eruptions can inject stratospheric sulfate aerosol into the atmosphere, which scatters the incoming solar radiation into the stratosphere, and plays a role in reducing the amount of solar radiation that reaches the surface (Robock 2000). Subsequently, the reduction of solar forcing caused by explosive volcanic eruptions is able to change the mean state of the tropical Pacific toward the El Niño-like warming from proxies (Handler 1984; Adams et al. 2003; D'Arrigo et al. 2009; Wilson et al. 2010; Shaheen et al. 2013) and modeling studies (Mann et al. 2005; Emile-Geay et al. 2008; McGregor et al. 2010; Landrum et al. 2013; Ohba et al. 2013). The paleo-climate data and a long term simulation of coupled ocean–atmosphere models indicate that the volcanic forcings influence the tropical Pacific Ocean in a manner similar to that of the period of solar irradiance minima (Santer et al. 2001; Gu and Adler 2011; Li et al. 2013). According to a recent study (Wang et al. 2012), the strong tropical volcanic eruptions accompanying large changes in the total solar irradiance play an important role in regulating the North Pacific decadal variability. Therefore, it is useful to examine how the natural external forcings, volcanic forcings in particular, are associated with SST changes in the tropical Pacific.

In this study, we examine the important question of how large of volcanic forcing can lead to El Niño-like warming in the tropical Pacific. While previous studies argued that a mechanism (i.e., feedback process) exists that can amplify the relatively small radiative forcings in order to produce the anomalous SST in the tropical Pacific, we further examine the existence of the threshold forcing of volcanic eruptions that lead to El Niño-like warming. In order to examine this issue, we analyze a millennium simulation (AD 1000–1990) forced by three external forcings including greenhouse gases (i.e., CO_2 and CH_4), solar forcing and volcanic eruptions.

The rest of this paper is organized as follows: Sect. 2 describes the model and the simulation employed in this study. In Sect. 3, the response of volcanic forcings with a different magnitude is examined based on the composite analysis. Finally, a summary and discussion is presented in Sect. 4, which also includes the result from the last millennium simulation of Paleoclimate Modeling Intercomparison Project Phase 3 (PMIP3) climate models.

2 ERIK simulation

The model used in this study is the ECHO-G coupled climate model (Legutke and Voss 1999), which consists of the spectral atmospheric model ECHAM4 (Roeckner et al. 1996) coupled with the global ocean circulation model HOPE-G (Wolff et al. 1997) using the OASIS coupler. Both of the models were developed and implemented at the Max Planck Institute for Meteorology in Hamburg and the description of the model physics and performance was referred to by Zorita et al. (2003). The configuration used for this simulation has 39 vertical levels, including 19 in the atmosphere and 20 in the ocean, and horizontal resolutions of 3.75° (atmosphere) and 2.8° (ocean) in both the latitude and longitude. The millennial integration for the period 1000–1990 AD includes a forced run (called ERIK) (Zorita et al. 2005), which was forced by three natural external forcing factors for annual resolution: solar forcing, greenhouse gas concentrations in the atmosphere including CO_2 and CH_4, and an estimated radiative effect of the stratospheric volcanic aerosols. In the ERIK simulation, the radiative flux at the top of the atmosphere is calculated to include the effects of sunspots and cosmic ray isotopes (Crowley 2000). Also, the effects of volcanic ash on radiation forcing is estimated first based on the concentration of sulfides in the Greenland ice core and then calculated by the atmospheric model (Robock and Free 1996). Note that the volcanic forcing in the ERIK simulation is parameterized as a simple reduction of the annual mean solar constant, starting in a year with a volcanic eruption and lasting 1 year (Liu et al. 2013). The concentration of CO_2 (Etheridge et al. 1996) and CH_4 (Blunier et al. 1995) are both integrated into the model based on the Antarctic ice core data.

Previous studies showed that the ERIK model reflects, to some extent, historical variations in the Northern Hemisphere temperature due to the changes in the natural external forcings and anthropogenic forcing in spite of some discrepancies (Mann 2007). In addition, it has been found that the ERIK simulation reasonably captures the simulated precipitation climatology, which is comparable to the Climate Prediction Center (CPC) Merged Analysis of Precipitation (CMAP) and the National Centers for Environmental Prediction (NCEP)-2 reanalysis data (Liu et al. 2009a, b). Also, the ECHO-G model well reproduced the ENSO phase-locking to the annual cycle and the subsurface ocean behavior related to equatorial wave dynamics (Min et al. 2005). Similar to the previous study (Min et al. 2005), the amplitude of the ENSO in the ERIK simulation is however too large and its occurrence is too regular (i.e., biennial timescales) (Fig. 1a, b). Note that one standard deviation of NINO3 (150°W–90°W, 5°N–5°S) SST index during the

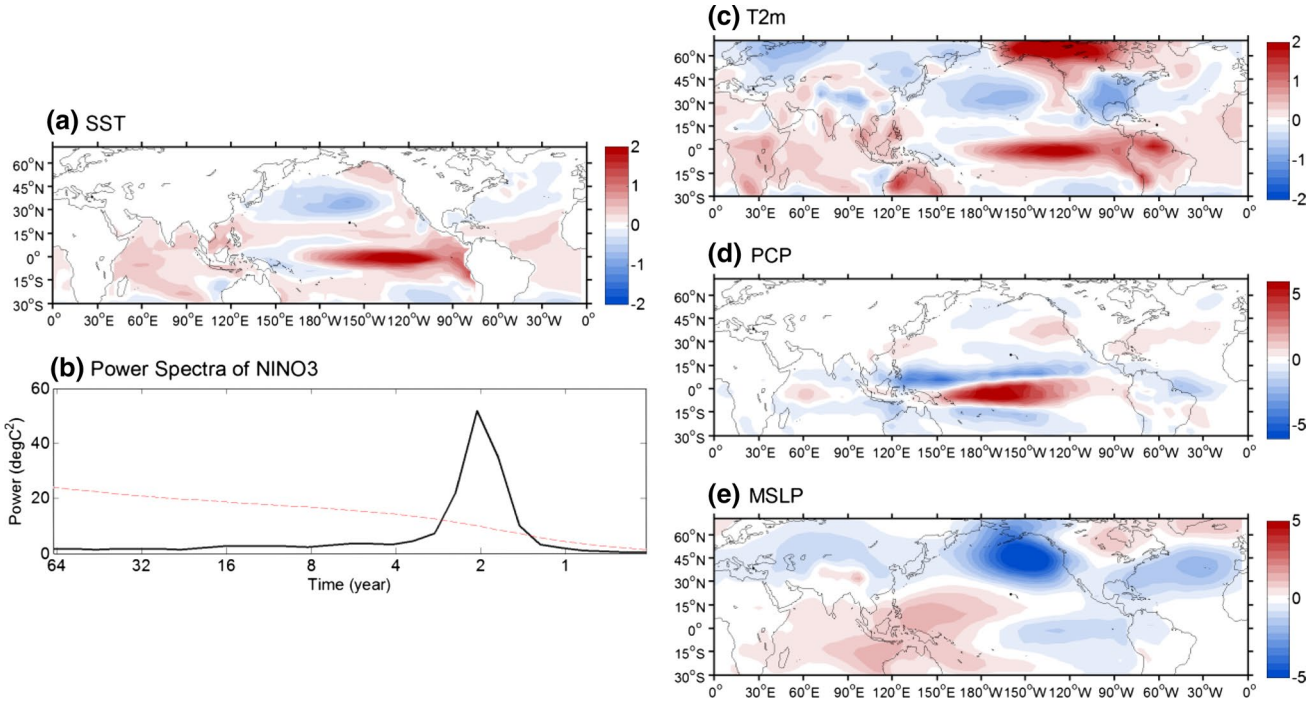

Fig. 1 *Left panels* are **a** the composited SST (°C) in El Niño events simulated in the ERIK and **b** the spectral density of the Nino3 SST index (*black*) with 95 % statistical confidence line (*red*). *Right panels* are the same as in (**a**) except (**c**) the near-surface temperature (°C) at 2 m, **d** precipitation (mm/day), and **e** sea level pressure (hPa). The El Niño event is defined when the NINO3 SST index during winter is above 1 °C in the ERIK simulation

boreal winter (Dec.–Jan.–Feb.) is 0.95 °C for 1950–2013 in the ERSST.v3 SST dataset (Smith et al. 2008), while that in the ERIK simulation is 1.53 °C for 1000–1990. Nevertheless, the ENSO-related teleconnection patterns including the near-surface temperature, precipitation and sea level pressure are reproduced realistically in the ERIK simulation (Fig. 1c–e). Therefore, it is still useful to examine the ERIK simulation to understand the influence of external forcing for a millennium time scale (Liu et al. 2013; Lim et al. 2014).

3 Results

In the ERIK simulation, the effective radiative forcing is used to represent the sum of the solar forcing (i.e., solar constant) and the volcanic forcing (Fig. 2a). A spike in the time series in Fig. 2a represents the effective radiative forcing in a year when a volcanic eruption occurs (see Fig. 2c). On the other hand, the carbon dioxide concentration, which is one of the most efficient greenhouse gases, remains fixed at approximately 270–280 ppm until the nineteenth century, after which it dramatically increases, especially after the mid-nineteenth century, to 350 ppm at the end of the twentieth century (Fig. 2b). In order to purposely exclude the effects of anthropogenic forcing, we pay attention to the period of 1000–1850 before the pre-industrial period when the natural external forcings (i.e., the solar forcing and the volcanic forcing) are dominant in the ERIK simulation.

Figure 2c shows the time series of the radiative forcing due to volcanic eruption (hereafter, we will refer to this as volcanic forcing) in the ERIK simulation for 1000–1850. The volcanic forcing occurred irregularly and the range between the maximum and minimum volcanic forcing is quite large at approximately 40 W/m^2. For example, the largest volcanic forcing occurred 1259 Samalas eruption in Indonesia (Lavigne et al. 2013), which is seven times larger than the scale of the Pinatubo volcanic forcing in 1991 (Kim and Kim 2012). Table 1 summarizes years when volcanic eruptions occurred. In order to conveniently examine the characteristics of the volcanic forcing response, we classify six different levels in the years when volcanic eruption occurred based on the magnitude of the volcanic forcing with an interval of 5 W/m^2. All of the 112 cases of volcanic forcing come under level 1 (52.7 %), level 2 (17.9 %), level 3 (16.0 %), level 4 (7.1 %), level 5 (4.5 %) and level 6 (1.8 %), respectively, during the last millennium.

In details, we also display the relationship between the NINO3 SST index during winter and the volcanic forcing with an interval 2 W/m^2 sliding composite for 1000–1850 (Fig. 3). Standard error is estimated by the sample estimate

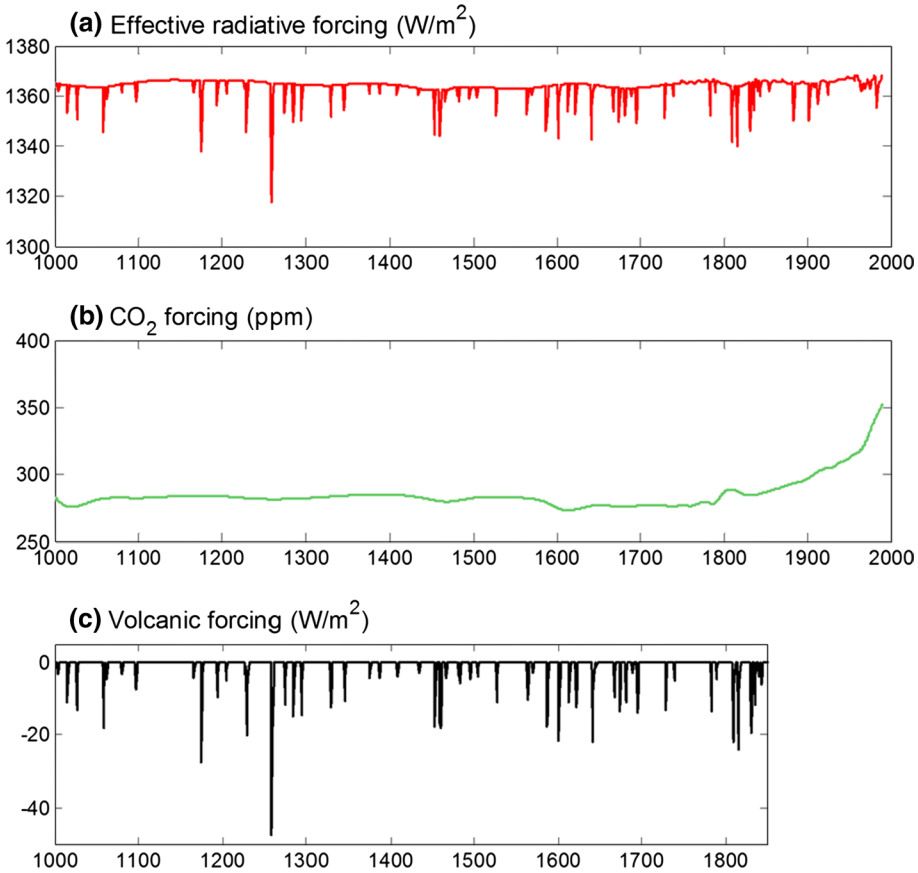

Fig. 2 The time series of **a** effective radiative forcing, **b** the concentration of carbon dioxide for 1000–1990 and **c** the radiative forcing due to volcanic eruption for 1000–1850 in the ERIK simulation. Unit is denoted in the upper part of each figure

Table 1 Year according to the magnitude of the volcanic forcing from level 1 to level 6 in the ERIK simulation

Group	Year (W/m^2)	Case number
Level 1 0 to −5 (W/m^2)	1027(4.8), 1062(4.8), 1495(4.8), 1589(4.8), 1675(4.8), 1789(4.8), 1830(4.8), 1166(4.4), 1276(4.4), 1330(4.4), 1375(4.4), 1387(4.4), 1466(4.4), 1623(4.4), 1836(4.4), 1016(4), 1177(4), 1346(4), 1408(4), 1481(4), 1504(4), 1528(4), 1565(4), 1614(4), 1682(4), 1840(4), 1195(3.6), 1668(3.6), 1004(3.2), 1080(3.2), 1227(3.2), 1643(3.2), 1811(3.2), 1817(3.2), 1689(3), 1098(2.8), 1231(2.8), 1434(2.8), 1570(2.8), 1603(2.8), 1844(2.4), 1206(2), 1063(1.6), 1167(1.6), 1376(1.6), 1388(1.6), 1409(1.6), 1467(1.6), 1496(1.6), 1505(1.6), 1645(1.6), 1790(1.6), 1841(1.6), 1005(1.2), 1081(1.2), 1228(1.2), 1435(0.8), 1571(0.8), 1646(0.4)	59
Level 2 −5 to −10 (W/m^2)	1194(9.68), 1667(9.68), 1816(8.8), 1602(8), 1642(8), 1810(8), 1230(7.6), 1097(7.4), 1832(7.2), 1059(6.8), 1461(6.8), 1261(6.4), 1454(6.4), 1843(6), 1286(5.6), 1483(5.6), 1205(5.2), 1296(5.2), 1696(5.2), 1739(5.2)	20
Level 3 −10 to −15 (W/m^2)	1295(14.52), 1695(14), 1674(13.48), 1783(13.48), 1729(13.28), 1026(13.08), 1588(12.64), 1329(12.52), 1622(12.4), 1275(11.8), 1835(11.8), 1015(11.16), 1527(11.16), 1613(11.16), 1681(11.16), 1345(10.6), 1564(10.48), 1176(10.4)	18
Level 4 −15 to −20 (W/m^2)	1831(19.44), 1460(18.12), 1058(18.04), 1587(17.88), 1260(17.6), 1453(17.6), 1459(16.8), 1285(15)	8
Level 5 −20 to −25 (W/m^2)	1815(23.92), 1641(22), 1809(22), 1601(21.72), 1229(20.36)	5
Level 6 Over −25 (W/m^2)	1259(47.28), 1175(27.76)	2

of the population standard deviation divided by the square root of the sample size. Figure 3 clearly shows that the NINO3 SST index during winter is above zero when the volcanic forcing is above 15 W/m^2, which is indicative of the threshold forcing to lead the El Niño-like warming in the ERIK simulation. Note that this result little changes when the interval of volcanic forcing changes from 1 to 5 W/m^2 with an increment of 1 W/m^2 (figure not shown).

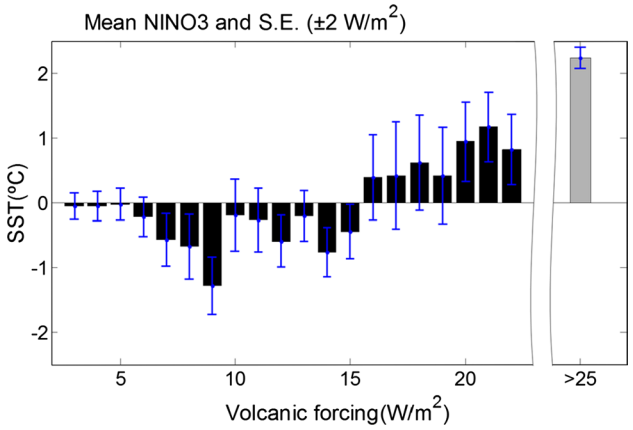

Fig. 3 The mean NINO3 SST index during winter with an interval 2 W/m^2 of volcanic forcing. The *bar* denotes the standard error in each interval. Note that the *last bar* indicates the NINO3 SST index above 25 W/m^2 of volcanic forcing

We further examine a composite of the anomalous SST at each level (from level 1 to level 6) in the tropical Pacific during winter (Fig. 4). Consistent with the result in Fig. 3, it is found that El Niño-like warming is apparently observed when the volcanic forcing is above level 4 (i.e., 15–20 W/m^2) (Fig. 4d–f). Again, this result indicates the existence of a threshold level of the volcanic forcing, which leads the El Niño-like warming in the ERIK simulation. We also display the seasonal evolution of the two composite SST in which volcanic forcing is below (level 1–3) and above (level 4–6) 15 W/m^2, respectively (Fig. 5). There is no El Niño-like warming throughout the year from the boreal spring (Mar.–Apr.–May, Fig. 5a), summer (Jun.–Jul.–Aug., Fig. 5b), and fall (Sept.–Oct.–Nov., Fig. 5c) to the winter (Fig. 5d) when the volcanic forcing is below 15 W/m^2. In contrast, when the volcanic forcing is above 15 W/m^2, the El Niño-like warming first appears during summer (i.e., the developing period,

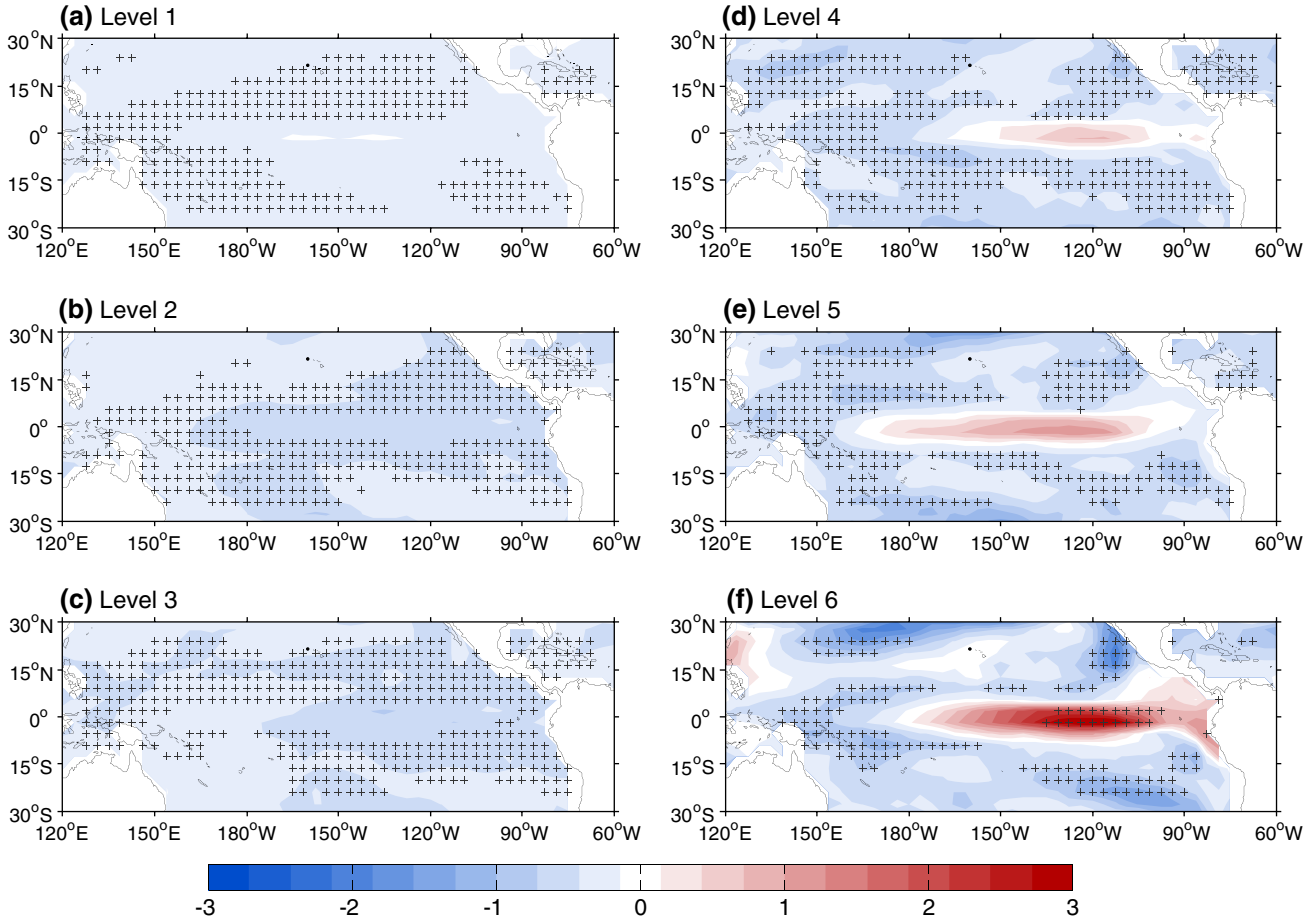

Fig. 4 The composite SST anomalies over the tropical Pacific Ocean in the groups of **a** level 1, **b** level 2, **c** level 3, **d** level 4, **e** level 5, and **f** level 6 during winter in the ERIK simulation. *Pluses* denote regions where the statistical significance level is above 95 %

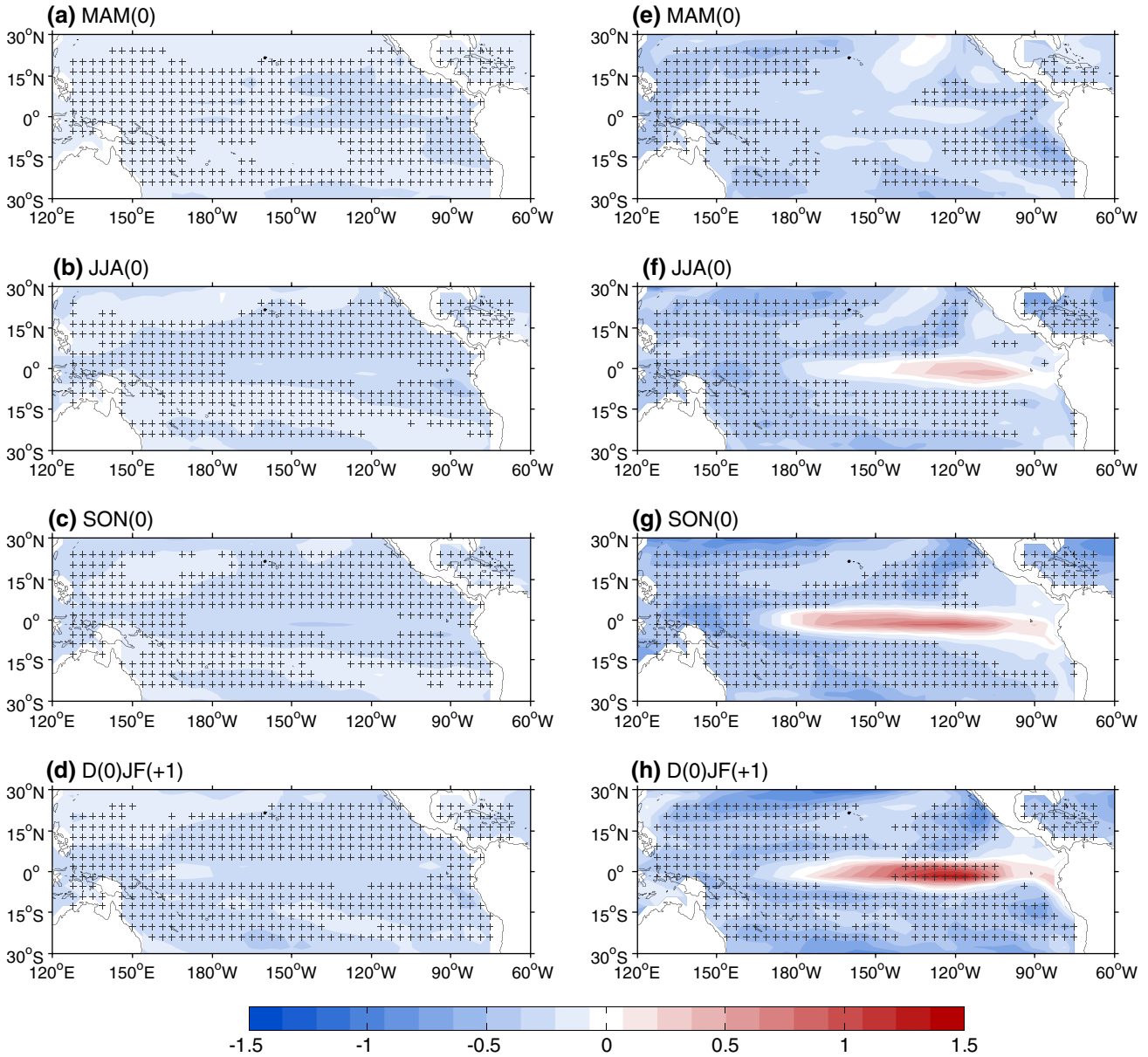

Fig. 5 The seasonal evolution of the composite anomalous SST from spring to winter when the volcanic forcing is below 15 W/m^2 (**a**–**d**) and when the volcanic forcing is above 15 W/m^2 (**e**–**h**). Note that any month in the volcanic eruption year is identified by the suffix (0) whereas any month in the following year of volcanic eruption by the suffix (+1). *Pluses* denote regions where the statistical significance level is above 95 %

Fig. 5f) and its intensity becomes stronger as the time progresses. The mature El Niño-like warming during winter (Fig. 5h) appears in the eastern tropical Pacific, which is statistically significant at a 95 % confidence level.

In order to examine the mechanism associated with the El Niño-like warming due to the threshold of volcanic forcing, we display the time evolution of the anomalous SST (Fig. 6a) and the low-level (850 hPa) zonal wind averaged within 2°N–2°S along the equator (Fig. 6b) from Jan. (0) to the next Apr. (+1) when the volcanic forcing is above 15 W/m^2. Before the El Niño-like warming reaches the mature stage around Nov. (0) and Dec. (0), the westerly appears in the western-to-central equatorial Pacific around Mar. (0)-to-Jun (0) (Fig. 6b). This westerly may act to reduce the trade winds that subsequently lead to El Niño-like warming during winter, which is mainly associated with the Bjerknes feedback processes (Bjerknes 1969). We further calculate the lead-lagged correlation coefficients between the NINO3 SST index and the anomalous zonal wind at 850 hPa averaged in the western equatorial Pacific (120°E–170°E, 5N°–5S°) from level 4 to level 6

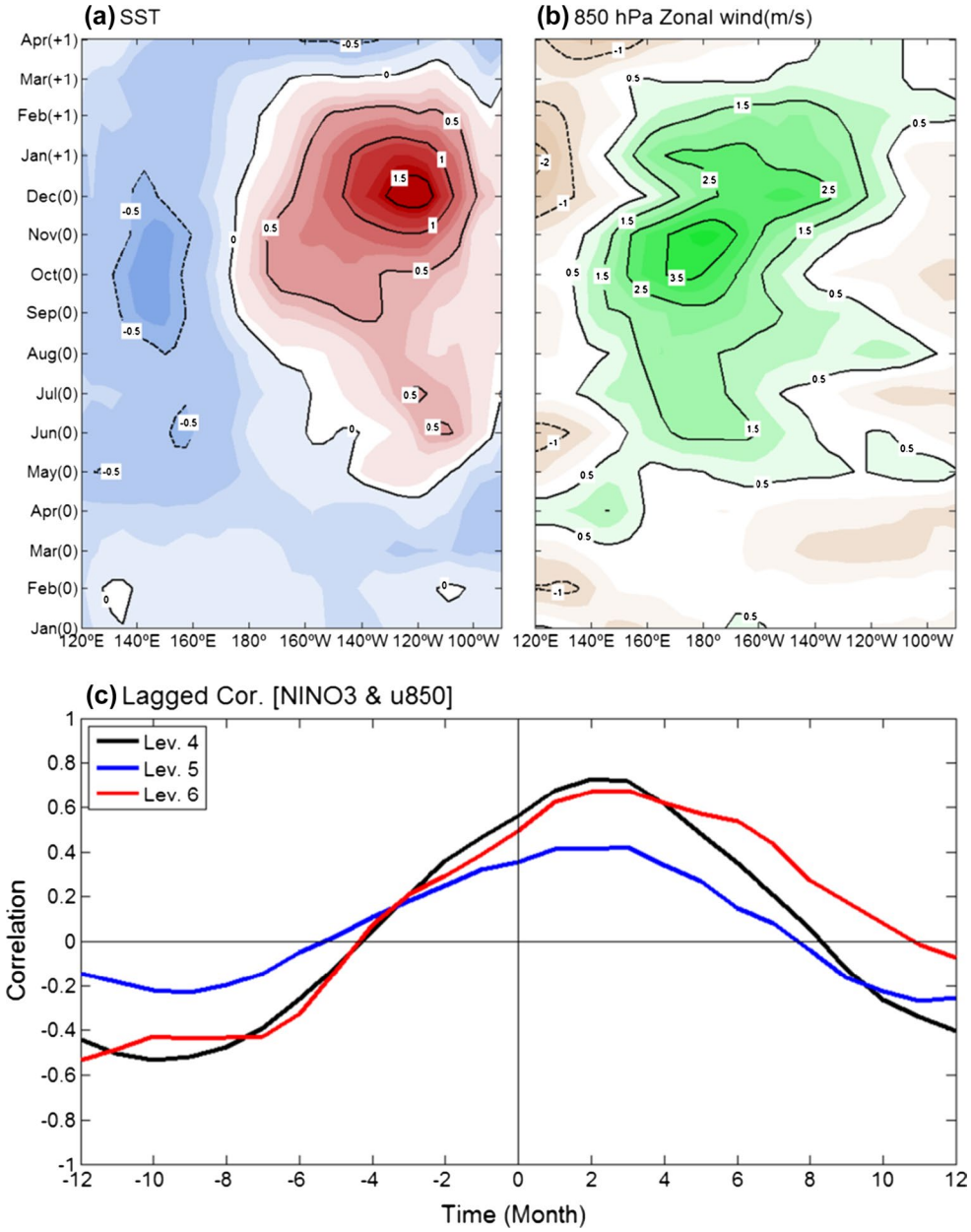

Fig. 6 The composite meridional mean structure (2N°–2S°) of the anomalous **a** SST, **b** 850 hPa zonal wind (m/s) from Jan. (0) to Apr. (+1) when the volcanic forcing is above 15 W/m^2. **c** the lead-lagged correlation between the NINO3 index (150°W–90°W, 5N°–5S°) and 850 hPa zonal wind in the western-to-central equatorial Pacific (120°E–170°E, 5N°–5S°). Note that any month in the volcanic eruption year is identified by the suffix (0) whereas any month in the following year of volcanic eruption by the suffix (+1)

(Fig. 6c). From level 4 to level 6, the maximum correlations are observed at lagged time of approximately 2–3 months, which is consistent with the results in Fig. 6a, b. Again, this indicates that the weakening of trade winds in the western-to-central equatorial Pacific leads the El Niño-like warming with a lagged time when the volcanic forcing is above 15 W/m^2.

To find the mechanism to cause a weakening of trade winds, the time evolution of the anomalous net surface shortwave radiation and SST in the subtropical Pacific (120°E–90°W, 15°N–30°N) along with the difference between evaporation (E) and precipitation (P) (i.e., E − P) from Jan. (0) to Apr. (+1) is shown in Fig. 7. Figure 7a shows that the averaged net surface shortwave radiation is low in the subtropical region for January to April, which is due to the volcanic eruption. It is evident that the subtropical Pacific SST with the volcanic forcing above 15 W/m^2 is cooler than that with the volcanic forcing below 15 W/m^2 (Fig. 7b). This is mostly due to the reduction in the net surface shortwave radiation caused by volcanic eruption (Fig. 7a). In particular, such a radiative forcing change is effective near the cloud-free areas in the subtropics (Meehl et al. 2008). Concurrently, a cool SST in the subtropical Pacific acts to decrease the amount of moisture evaporating into the atmosphere, leading the reduction of E − P when the volcanic forcing is above 15 W/m^2 (Fig. 7c). It is evident that the reduction of E − P is able to cause a weakening of ITCZ (Fig. 8) and such a phenomenon is also associated with a weakening of trade winds, subsequently, a southward shift of the ITCZ position. Therefore, this result may explain why the volcanic

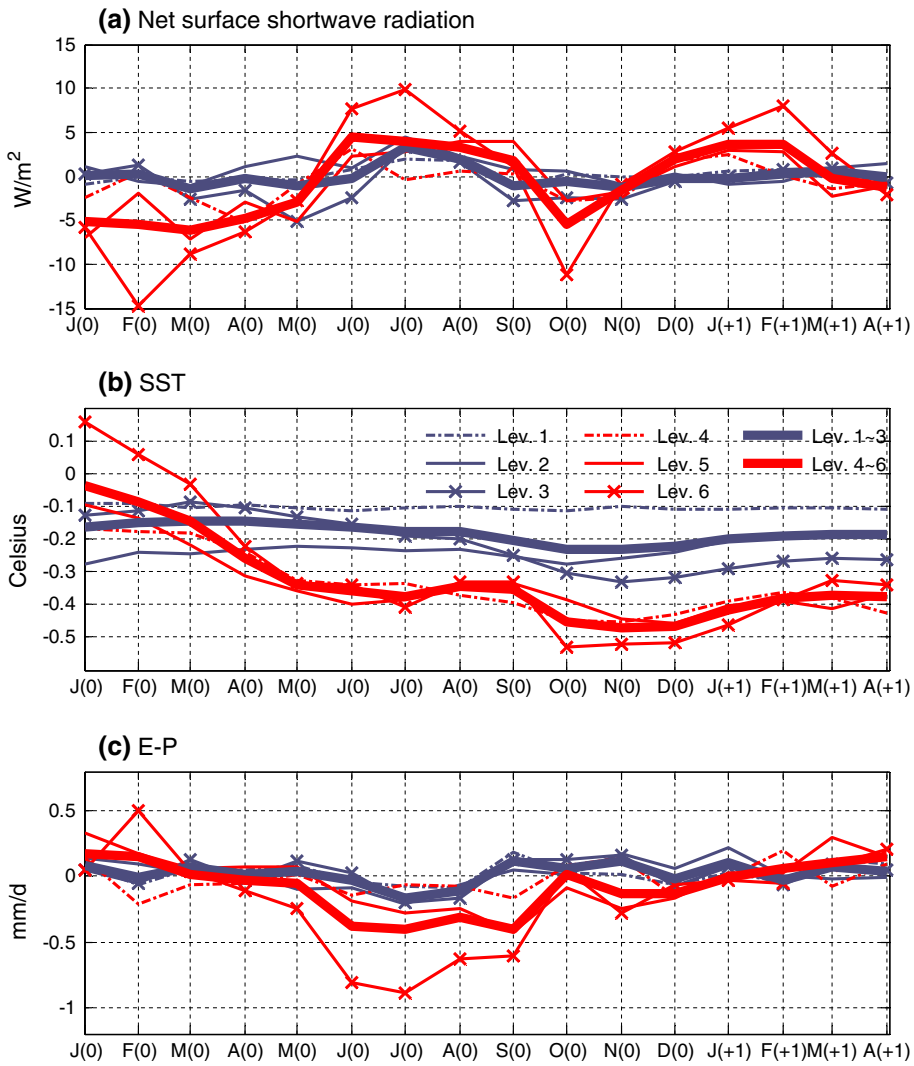

Fig. 7 The composite time evolution of the anomalous. **a** Net surface shortwave radiation, **b** SST, and **c** difference between evaporation (E) and precipitation (P) (i.e., E − P) in the subtropical Pacific (120°E–90°W, 15°N–30°N) from Jan. (0) to Apr. (+1) from level 1 to level 6. *Thick blue* and *red lines* denote the averaged net surface shortwave radiation in (**a**), SST in (**b**), and E − P in (**c**) when the volcanic forcing is below and above 15 W/m^2, respectively

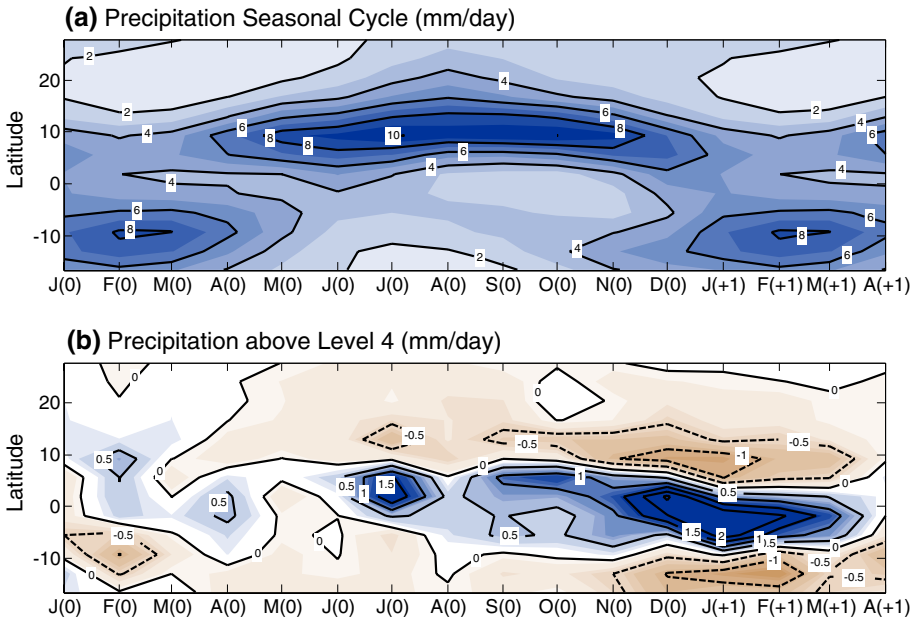

Fig. 8 **a** The zonal (120°E–90°W) mean climatological seasonal cycle of precipitation in the ERIK simulation and **b** the composite anomalous precipitation averaged in the tropical Pacific basin (120°E–90°W) from Jan. (0) to Apr. (+1) when the volcanic forcing is above 15 W/m^2

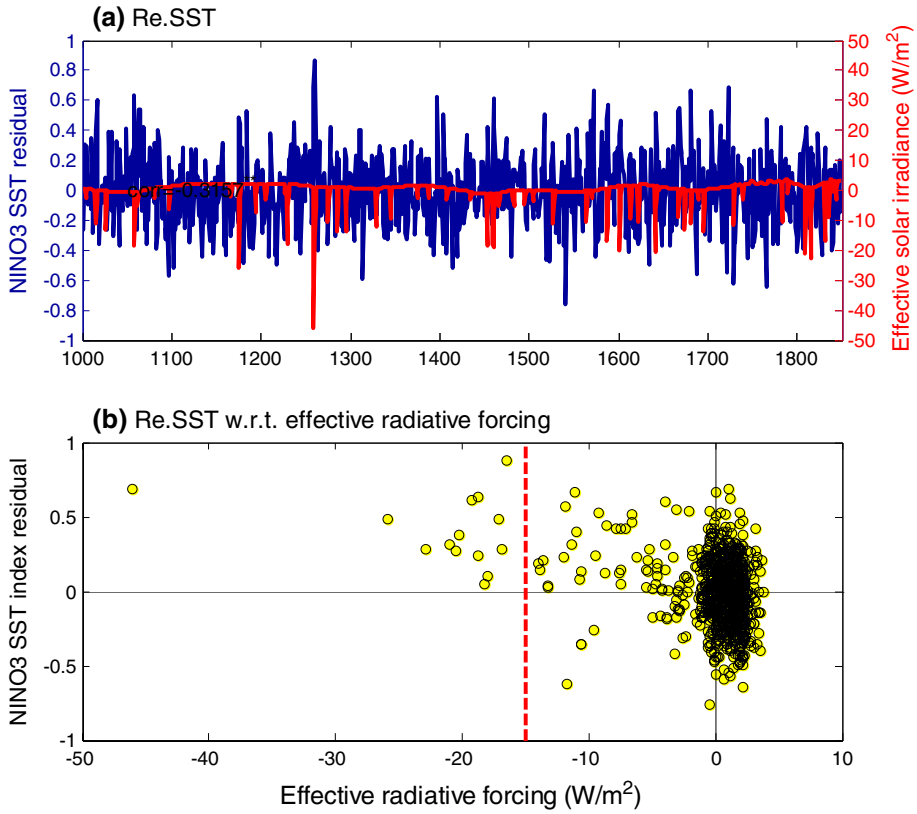

Fig. 9 **a** Time series of residual NINO3 SST index (*blue*) and effective solar irradiance anomaly (*red*). **b** Scatter plot of the residual NINO3 SST index and the effective radiative forcing. *Red dashed line* in **b** indicates −15 W/m^2. See the text for the definition of the residual NINO3 SST index

forcing above 15 W/m^2 is a critical threshold forcing to lead the El Niño-like warming. We argue that the threshold forcing above 15 W/m^2 is able to cool the subtropical ocean leading the weakening of ITCZ through the modulation of E and P, subsequently, a weakening of trade winds.

Figure 8a displays the climatological seasonal cycle of the zonal mean (120°E–90°W) precipitation in the ERIK simulation. It is evident that the climatological ITCZ in the ERIK simulation, which is located off the equator around 10°N, is prominent from Apr. to Dec. in the Northern Hemisphere. Figure 8b is the same as Fig. 8a except the composite anomalous precipitation from Jan. (0) to Apr. (+1) when the volcanic forcing is above 15 W/m^2. The intensity of the ITCZ around 5°N–10°N becomes weak around Mar. (0)-to-Jun. (0). In addition, it is evident that the position of ITCZ is shifted to the south as discussed above. It should be noted that there is little change in the ITCZ when the volcanic forcing is below 15 W/m^2 (not shown).

To further support the notion that the volcanic forcing above 15 W/m^2 may be a threshold radiative forcing to lead the El Niño-like warming, we examine the relationship of the effective solar irradiance and the anomalous warming in the eastern tropical Pacific without El Niño event in the ERIK simulation. We first calculate the first empirical orthogonal function (EOF1) SST representing the ENSO along with its principal component (PC) time series in the ERIK simulation (not shown figure). Note that the EOF1 explains a large variance of the total SST variability (i.e., 55.6 %) and the PC time series is highly correlated with the NINO3 SST Index (i.e., r = 0.98, here, r is a simultaneous correlation coefficient). And then, we obtain the residual SST anomalies by subtracting the reconstructed SST anomalies from the total SST anomalies by the EOF1 and PC time series. Figure 9a shows the residual NINO3 SST index, which is defined as the residual SST anomalies averaged in the NINO3 region, along with the time series of effective solar irradiance. A simultaneous correlation coefficient between the two time series is −0.33, which is statistically significant at the 95 % confidence level. That is, the reduction of effective solar irradiance due to the volcanic forcing is associated with a warming in the eastern tropical Pacific without El Nino event. Figure 9b displays the scatter plot between the residual NINO3 index and the effective solar irradiance. It is evident that the residual SST is always above zero when the effective solar irradiance is above around 15 W/m^2, indicating that the radiative forcing above 15 W/m^2 may be a threshold forcing to lead the anomalous warming in the eastern tropical Pacific.

4 Summary and discussion

There is an agreement among researchers that both solar forcing and volcanic forcing play a role in initiating the

Table 2 The PMIP3 climate models used in the present study

Institute	Model ID	Volcanic forcing	Solar forcing
NCAR	CCSM4	Gao et al. (2008)	Vieira et al. (2011)
LASG-IAP	FGOALS-s2	Gao et al. (2008)	Vieira et al. (2011) and Wang et al. (2005)
MRI	MRI-CGCM3	Gao et al. (2008)	Delaygue and Bard (2011) and Wang et al. (2005)
BCC	BCC-CSM1-1	Gao et al. (2008)	Vieira et al. (2011) and Wang et al. (2005)

anomalous warm/cold SST in the tropical Pacific through feedback processes. However, there is no consensus on the existence of threshold forcing that leads to El Niño-like warming. In order to examine this issue, we analyze a millennium ERIK simulation (AD 1000–1850) forced by three natural external forcings including greenhouse gases, solar forcing and volcanic eruptions.

The volcanic forcing occurs irregularly and the range between the maximum and minimum volcanic forcing is quite large at approximately 40 W/m^2 in the ERIK simulation. The composite analysis reveals that the El Niño-like warming can be observed when the volcanic forcing is above the threshold forcing, i.e., 15 W/m^2 in the ERIK simulation. By analyzing SST, low-level winds, evaporation and precipitation, we examined a possible mechanism how the volcanic forcing above 15 W/m^2 is able to lead the El Niño-like warming in the ERIK simulation. The westerly appears in the western equatorial Pacific during the spring and the early summer, and it is able to lead the El Niño-like warming during the following winter through the Bjerknes feedback processes. We argued that the air–sea coupled processes play a key role to weaken the trade winds. That is, the reduction in the radiative forcing due to volcanic eruptions effectively leads a cooling in the subtropical Pacific where the total amount of cloud is less. Subsequently, a cool SST in the subtropical Pacific acts to decrease the amount of moisture evaporating into the atmosphere, which is associated with the weakening of the ITCZ by a reduced moisture advection from the subtropical Pacific to the ITCZ. A weakening of the ITCZ is also associated with a weakening of trade winds, concurrently, a southward shift of the ITCZ position.

In the present study, we emphasize that the volcanic eruption above the threshold forcing (i.e., 15 W/m^2) is able to change the state of tropical Pacific along with the modulation of the ITCZ. It is important to know how large of external natural forcing is able to influence natural variability such as ENSO. Knowing this critical threshold forcing could be also useful to examine how large of anthropogenic forcing is able to modify natural variability. For example, if we know the exact threshold radiative forcing due to external forcing and/or anthropogenic forcing to modify natural variability, it would be very useful to build the adaption plan to cope with climate change. In other words, the change in the radiative forcing, which is due to either the anthropogenic forcing or the natural external forcing, should be above a certain level of threshold value to modulate climate system. On the other hand, it should be acknowledged that the critical threshold of the volcanic forcing 15 W/m^2 includes the effects of solar, volcanic and GHG forcing simultaneously, therefore, if the solar constant and GHG change more, the critical threshold may change accordingly. Furthermore, the ERIK simulation is not able to distinguish the importance of sites and volcanic eruption month, thereby the volcanic forcing is constantly added in effective solar radiation for 1 year.

In addition, the present study uses only a single model (i.e., ERIK simulation) to examine the existence of the threshold of volcanic forcing. Therefore, it would be valuable to examine whether other climate models or proxy data have the threshold of the volcanic forcing to lead the El Niño-like warming. Using the proxies around 500 years ago, previous studies argued that there is a good agreement that a strong volcanic eruptions are significantly responsible for the El Niño-like warming (Adams et al. 2003; D'Arrigo et al. 2009; Wilson et al. 2010). We also briefly analyze the last millennium simulation of PMIP3 climate models (BCC-CSM1-1, FGOALS-s2, MRI-CGCM3, and CCSM4) in which the concentration of sulfate aerosol due to the volcanic eruptions is prescribed by following Gao et al. (2008) (Table 2). Note that the sulfate aerosol concentration due to volcanic eruptions is obtained from 54 ice core records from both the Arctic and Antarctica (Fig. 10a). First of all, it should be acknowledged that the effect of volcanic eruptions is differently prescribed in the PMIP3 simulation (i.e., sulfate aerosol concentration) and the ERIK simulation (i.e., effective radiative forcing). Therefore, it is difficult to directly compare with the results from the PMIP3 and ERIK simulations. Figure 10b displays the NINO3 SST index from the PMIP3 climate models along with their ensemble mean at the level of sulfate aerosol concentration. It is found that the El Niño-like warming is apparently observed when the concentration of sulfate aerosol is above 50 Tg, which is indicative of the existence of threshold forcing to lead the El Niño-like warming in the PMIP3 simulation. Note that the NINO3 SST index is below zero when the concentration of sulfate aerosol is above 100 Tg. This is mostly due to huge tropical volcanic eruptions occurred during the Medieval

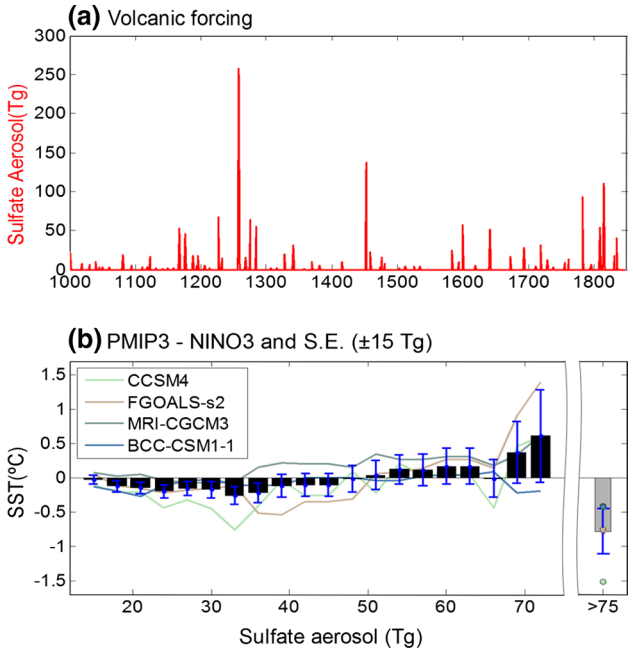

Fig. 10 **a** Volcanic forcings represented by the concentration of sulfate aerosol in the last millennium simulation of PMIP3 climate models (Gao et al. 2008). **b** The NINO3 SST index during winter in the PMIP3 climate models (BCC-CSM1-1, FGOALS-s2, MRI-CGCM3, and CCSM4) (*contour*) with their ensemble mean (*black bar*) in the interval 15 Tg of sulfate aerosol concentration. Note that the *last bar* in **b** indicates the NINO3 SST index above 75 Tg of sulfate aerosol concentration. The *vertical bars* denote the standard error in each interval

climatic Anomaly, which is characterized by strong La Niña-like tropical Pacific mean state (Mann et al. 2009; Lewis and LeGrande 2015). However, Fig. 10a also shows that the huge volcanic eruptions (>100 Tg) occurred not only in the Medieval Warm Period, but also in the Little Ice Age and Present Warm Period. It is found that the NINO3 SST index is negative in all PMIP3 climate models when the volcanic eruptions occurred during the Medieval climatic Anomaly (not shown). However, there is inconsistency among PMIP3 climate models when the volcanic eruption occurred during the Little Ice Age and Present Warm Period, which may partly support the previous hypothesis (Lewis and LeGrande 2015). In spite of this, we cannot exclude another possibility that volcanic forcing play an important role in the transition of El Nino-like SST to La Nina-like SST.

Acknowledgments This study was funded by the Korea Ministry of Environment (MOE) as "Climate Change Correspondence Program". S.-W. Yeh is also supported from the Brain Korea 21 Plus Project in Department of Marine Sciences and Convergent Technology of Hanyang University. H.-G. Lim is supported by the Human Resources Development of the Korea Institute of Energy Technology Evaluation and Planning (KETEP) grant funded by the Korea government Ministry of Trade, industry & Energy (No. 20144030200460) and Hyundai Motor Chung Mong-Koo Foundation as well. Y.-G. Park and J.-H. Park are supported from KIOST in-house grants (PE99291, PE99293).

References

Adams BJ, Mann ME, Ammann CM (2003) Proxy evidence for an El Niño-like response to volcanic forcing. Nature 426:274–278. doi:10.1038/nature02101

Alexander MA, Blade I, Newman M, Lanzante JR, Lau NC, Scott JD (2002) The atmospheric bridge: the influence of ENSO teleconnections on air–sea interaction over the global oceans. J Clim 15:2205–2231. doi:10.1175/1520-0442(2002)015<2205:TABTIO>2.0.CO;2

Battisti DS, Hirst AC (1989) Interannual variability in a tropical atmosphere–ocean model: influence of the basic state, ocean geometry and nonlinearity. J Atmos Sci 46:1687–1712. doi:10.1175/1520-0469(1989)046<1687:IVIATA>2.0.CO;2

Bjerknes J (1969) Atmospheric teleconnections from the equatorial pacific. Mon Weather Rev 97:163–172

Blunier T, Chappellaz J, Schwander J, Stauffer B, Raynaud D (1995) Variations in atmospheric methane concentration during the Holocene epoch. Nature 374:46–49. doi:10.1038/374046a0

Burgers G, Jin FF, van Oldenborgh GJ (2005) The simplest ENSO recharge oscillator. Geophys Res Lett 32:L13706. doi:10.1029/2005GL022951

Crowley TJ (2000) Causes of climate change over the past 1000 years. Science 289:270–277

D'Arrigo R, Wilson R, Tudhope A (2009) The impact of volcanic forcing on tropical temperatures during the past four centuries. Nat Geosci 2:51–56. doi:10.1038/NGEO393

Delaygue G, Bard E (2011) An Antarctic view of Beryllium-10 and solar activity for the past millennium. Clim Dyn 36(11–12):2201–2218. doi:10.1007/s00382-010-0795-1

Emile-Geay J, Seager R, Cane MA, Cook ER, Haug GH (2008) Volcanoes and ENSO over the past millennium. Am Meteorol Soc 21:3134–3148

Etheridge DM, Steele LP, Langenfelds RL, Francey RJ, Barnola JM, Morgan VI (1996) Natural and anthropogenic changes in atmospheric CO_2 over the last 1000 years from air in Antarctic ice and firn. J Geophys Res 101:4115–4128. doi:10.1029/95JD03410

Gao C, Robock A, Ammann C (2008) Volcanic forcing of climate over the past 1500 years: an improved ice core-based index for climate models. J Geophys Res 113(D23):D23111. doi:10.1029/2008JD010239

Gu G, Adler RF (2011) Precipitation and temperature variations on the interannual time scale: assessing the impact of ENSO and volcanic eruptions. Am Meteorol Soc 24:2258–2270

Handler P (1984) Possible association of stratospheric aerosols and El Nino type events. Geophys Res Lett 11:1121–1124

Jin FF (1997) An equatorial ocean recharge paradigm for ENSO. Part I: conceptual model. J Atmos Sci 54:811–829

Kim SJ, Kim BM (2012) Ocean response to the pinatubo and 1259 volcanic eruptions. Ocean Polar Res 34(3):305–323. doi:10.4217/OPR.2012.34.3.305

Landrum L, Otto-Bliesner BL, Wahl ER, Conley A, Lawrence PJ, Rosenbloom N, Teng H (2013) Last millennium climate and its variability in CCSM4. J Clim 26:1085–1111

Lau NC (1997) Interactions between global SST anomalies and the mid-latitude atmospheric circulation. Bull Am Meteorol Soc 78:21–33. doi:10.1175/1520-0477(1997)078<0021:IBGSAA>2.0.CO;2

Lavigne F et al (2013) Source of the great AD 1257 mystery eruption unveiled, Samalas volcano, Rinjani Volcanic Complex, Indonesia. PNAS 110:16742–16747
Legutke S, Voss R (1999) The Hamburg atmosphere–ocean coupled circulation model ECHO-G. German Climate Computer Center (DKRZ) Tech Rep 18
Lewis SC, LeGrande AN (2015) Stability of ENSO and its tropical Pacific teleconnections over the last millennium. Clim Past Discuss 11:1579–1613. doi:10.5194/cpd-11-1579-2015
Li J et al (2013) El Nino modulations over the past seven centuries. Nat Clim Change. doi:10.1038/NCLIMATE1936
Lim HG, Yeh SW, Kim JW, Park R, Song CK (2014) Contributions of solar and greenhouse gases forcing during the present warm period. Meteorol Atmos Phys. doi:10.1007/s00703-014-0324-6
Liu J, Wang B, Ding Q, Kuang X, Soon W, Zorita E (2009a) Centennial variations of the global monsoon precipitation in the last millennium: results from ECHO-G model. J Clim 22:2356–2371. doi:10.1175/2008JCLI2353.1
Liu J, Wang B, Wang H, Kuang X, Ti R (2009b) Forced response of the East Asian summer rainfall over the past millennium: results from a coupled model simulation. Clim Dyn. doi:10.1007/s00382-009-0693-6
Liu J, Wang B, Cane MA, Yim SY, Lee JY (2013) Divergent global precipitation changes induced by natural versus anthropogenic forcing. Nature. doi:10.1038/nature11784
Mann ME (2007) Climate over the past two millennia. Annu Rev Earth Planet Sci 35:111–136. doi:10.1146/annurev.earth.35.031306.140042
Mann ME, Cane MA, Zebiak SE, Clement A (2005) Volcanic and solar forcing of the tropical Pacific over the past 1000 years. J Clim 18:447–456
Mann ME, Zhang Z, Rutherford S, Bradley RS, Hughes MK, Shindell D, Ammann C, Faluvegi G, Ni F (2009) Global signatures and dynamical origins of the little ice age and medieval climate anomaly. Science 326:1256–1260. doi:10.1126/science.1177303
McGregor S, Timmermann A, Timm O (2010) A unified proxy for ENSO and PDO variability since 1650. Clim Past 6:1–17
McPhaden MJ, Zebiak SE, Glantz MH (2006) ENSO as an integrating concept in Earth science. Science 314(5806):1740–1745. doi:10.1126/science.1132588
Meehl GA, Washington WM, Wigley TML, Arblaster JM, Dai A (2003) Solar and greenhouse gas forcing and climate response in the 20th century. J Clim 16:426–444
Meehl GA, Arblaster JM, Branstator G, van Loon H (2008) A coupled air–sea response mechanism to solar forcing in the Pacific region. Am Meteorol Soc 21:2883–2897
Meehl GA, Arblaster JM, Matthes K, Sassi F, van Loon H (2009) Amplifying the pacific climate system response to a small 11-year solar cycle forcing. Science 325:1114–1118. doi:10.1126/science.1172872
Min SK, Legutke S, Hense A, Kwon WT (2005) Internal variability in a 1000-yr control simulation with the coupled climate model ECHO-G—II. El Nino Southern Oscillation and North Atlantic Oscillation. Tellus 57A:622–640
Ohba M, Shiogama H, Yokohata T, Watanabe M (2013) Impact of strong tropical volcanic eruptions on ENSO simulated in a coupled GCM. J Clim 26:5169–5182. doi:10.1175/JCLI-D-12-00471.1
Picaut J, Masai F, du Penhoat Y (1997) An advective–reflective conceptual model for the oscillatory nature of the ENSO. Science 277(5326):663–666. doi:10.1126/science.277.5326.663
Robock A (2000) Volcanic eruptions and climate. Rev Geophys 38(2):191–219
Robock A, Free M (1996) The volcanic record in ice cores for the past 2000 years. In: Jones P, Bradley R, Jouzel J (eds) Climatic variations and forcing mechanisms of last 2000 years. Springer, New York, pp 533–546
Robock A, Mao J (1995) The volcanic signal in surface temperature observations. J Clim 8:1086–1103
Roeckner E, Oberhuber JM, Bacher A, Christoph M, Kirchner I (1996) ENSO variability and atmospheric response in a global coupled atmosphere–ocean GCM. Clim Dyn 12(11):737–754
Santer BD et al (2001) Accounting for the effects of volcanoes and ENSO in comparisons of modeled and observed temperature trends. J Geophys Res 106(D22):28033–28059
Schopf PS, Suarez MJ (1988) Vacillations in a coupled ocean–atmosphere model. J Atmos Sci 45:549–566. doi:10.1175/1520-0469(1988)045<0549:VIACOM>2.0.CO;2
Shaheen R, Abauanza M, Jackson TL, McCabe J, Savarino J, Thiemens MH (2013) Tales of volcanoes and El-Niño southern Oscillations with the oxygen isotope anomaly of sulfate aerosol. PNAS 110(44):17662–17667
Smith TM, Reynolds RW, Peterson TC, Lawrimore J (2008) Improvements NOAAs historical merged land-ocean temp analysis (1880–2006). J Clim 21:2283–2296
Suarez MJ, Schopf PS (1988) A delayed action oscillator for ENSO. J Atmos Sci 45:3283–3287. doi:10.1175/1520-0469(1988)045<3283:ADAOFE>2.0.CO;2
van Loon H, Meehl GA (2008) The response in the pacific to the sun's decadal peaks and contrasts to cold events in the southern oscillation. J Atmos Solar Terr Phys 70:1046–1055
van Loon H, Meehl GA, Arblaster JM (2004) A decadal solar effect in the tropics in July–August. J Atmos Sol Terr Phys 66:1767–1778. doi:10.1016/j.jastp.2004.06.003
van Loon H, Meehl GA, Shea DJ (2007) Coupled air–sea response to solar forcing in the pacific region during northern winter. J Geophys Res 112:D02108
Vecchi GA, Soden BJ, Wittenberg AT, Held IM, Leetmaa A, Harrison MJ (2006) Weakening of tropical Pacific atmospheric circulation due to anthropogenic forcing. Nature. doi:10.1038/nature04744
Vieira LEA, Solanki SK, Krivova NA, Usoskin I (2011) Evolution of the solar irradiance during the Holocene. Astron Astrophys 531:A6. doi:10.1051/0004-6361/201015843
Vimont DJ, Battisti DS, Hirst AC (2001) Footprinting: a seasonal connection between the tropics and mid-latitudes. Geophys Res Lett 28(20):3923–3926. doi:10.1029/2001GL013435
Wang Y, Lean J, Sheeley NS Jr (2005) Modeling the Sun's magnetic field and irradiance since 1713. Astrophys J 625:522–538
Wang T, Ottera OH, Gao Y, Wang H (2012) The response of the North Pacific decadal variability to strong tropical volcanic eruptions. Clim Dyn 39(12):2917–2936
Wilson R, Cook E, D'Arrigo R, Riedwyl N, Evans MN, Tudhope A, Allan R (2010) Reconstructing ENSO: the influence of method, proxy data, climate forcing and teleconnections. J Q Sci 25:62–78. ISSN 0267-8179
Wolff JO, Maier-Reimer E, Legutke S (1997) The Hamburg ocean primitive equation model HOPE. Technical Report 13. German Climate Computer Center (DKRZ) Hamburg, Germany
Zorita E, Gonzalez-Rouco F, Legutke S (2003) Testing the Mann et al. (1998) Approach to paleoclimate reconstructions in the context of a 1000-yr control simulation with the ECHO-G coupled climate model. J Clim 16:1378–1390. doi:10.1175/1520-0442(2003)16<1378:TTMEAA>2.0.CO;2
Zorita E, Gonzalez-Rouco JF, von Storch H, Montavez JP, Valero F (2005) Natural and anthropogenic modes of surface temperature variations in the last thousand years. Geophys Res Lett. doi:10.1029/2004GL021563